

Uncalibrated Image-based Position-Force Adaptive Visual Servoing for Constrained Robots under Dynamic Friction Uncertainties*

E.C. Dean-León, L.G. García-Valdovinos and V. Parra-Vega
Mechatronics Division, CINVESTAV-IPN
IPN 2508, Sn P. Zacatenco, México, D.F., 7300. México
{edean, lgarcia, vparra}@cinvestav.mx

A. Espinosa-Romero
Faculty of Mathematics, Universidad Autónoma de Yucatán
Mérida, Yucatán. México
eromero@tunku.uady.mx

Abstract—Visual servoing of constrained dynamical robots has not yet met a formal treatment. Also, notices that due technological constraints, this tasks is done slowly at velocity reversals, thus dynamic friction arises, which complicates even more the problem. In this paper, a new adaptive scheme for visual servoing of constrained robots subject to dynamic friction is proposed. An image-based control is introduced to produce simultaneous convergence of the constrained *visual position* and the contact force between the end-effector and the constraint surface. Camera and robot parameters are considered uncertain. This new approach is based on a new formulation of the orthogonalization principle used in force control, coined here *visual orthogonalization principle*. This allows, under the framework of passivity, to yield a synergetic scheme that fuses camera, encoder and force sensor signals. Simulations results are presented and shows that image errors and force errors converge despite uncertainties of friction model.

Index Terms—Visual Servoing, Adaptive Force Control, Sensor Fusion, Dynamic Friction.

I. INTRODUCTION

Robot tasks that involve joint encoders, force sensors, CCD cameras, proximity sensors, haptic interfaces, and tactile devices pose a challenging problem in robotics due to the multisensor/multisampling nature of the problem. However, it is well known that multisensor-based robot control approaches may offer a solution to very important and relevant, but complex, problems in robotics. In order to achieve sensor fusion-based controller, a careful analysis of the dynamics, sensors behavior, and tasks are required. Furthermore, since physical parameters are in practice uncertain, robustness to parametric uncertainties, are an integral part of the control problem. One of such tasks is the force-position control of a robot using visual information. In this paper, we focus in the following problem: “*design a controller that ensures tracking of image based trajectories of constrained robots subject to uncertainties on camera, robot and dynamic friction parameters*”. This problem has been elusive because it is not evident how to deal with vision and force signals, despite lot of the availability of schemes of vision or force.

*This work is supported by CONACyT under doctoral scholarship #158973, #158613, and project #39727-Y

A. Motivation

The task under study is that the robot end effector tracks a *visual* trajectory along the surface of an object, and at the same time, control the applied force exerted in the surface by the end-effector, see Figure (1). This task is very relevant in many robotic applications. However, for any practical impact, uncertainties must be considered.

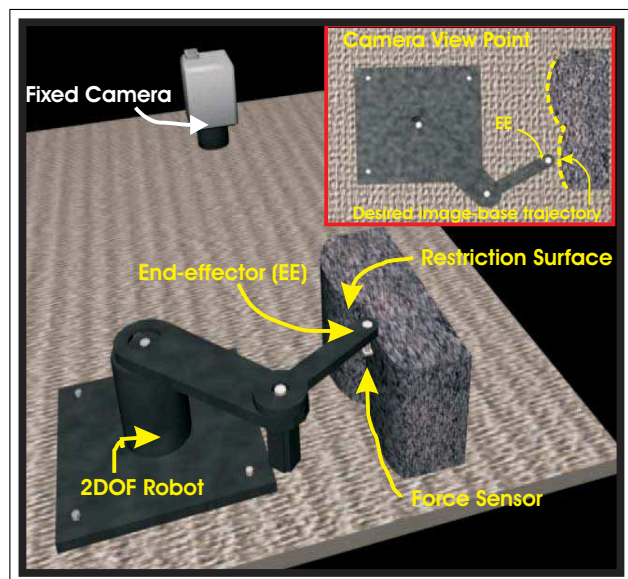


Fig. 1. Robot Force-Vision System

On the other hand, joint friction is quite important to compensate because it is a dominant dynamical force in slow and velocity reversal regimes. Therefore, we consider the LuGre model¹, which reproduces pre-sliding regime at very small displacements and hard nonlinearities for slow motion and velocity reversals, which is *typical motion regime of contact tasks*. Interestingly, we derive a friction compensator that depends on image errors.

¹This dynamic friction is responsible for limit cycles.

B. Contribution

An adaptive controller driven by image errors and contact force errors is proposed to solve by first time the problem posed above. The underlying reason that allows to obtain this result is that a new image-based error manifold is introduced to propose a visual-based orthogonalized principle. Thus, similar results to the case of nonvisual-based orthogonalized principle are obtained. This nontrivial extension, allows to solve formally this problem, and the closed-loop system guarantees exponential tracking of position and force trajectories subject to parametric uncertainties. This scheme delivers a smooth controller and presents formal stability proofs. Simulations allows to visualize the expected closed loop performance predicted by the theory. We further extend our proposal to include visual compensation of dynamic friction. Surprisingly the control structure is quite simple, in contrast, the proof is rather involved, though straightforward.

II. BACKGROUND

Hybrid vision/force control approaches have been reported [1], [2], [3], [4], and none of them shows robustness to uncertainties, on robot parameters and camera parameters. In a different path, the authors Xiao et al. [5], present an interesting scheme of hybrid vision force control in an uncalibrated environment, but their approach does not deal with uncertainties of robot parameters, and exhibits a very complex control law. Finally, the authors [13] present a novel concept using a neural network in order to adapt the unknown robot parameters for constrained robots, but that sort of schemes are out of the scope of this work.

With respect to force control, Arimoto solved by first time the simultaneous control of position and force using the full nonlinear dynamics subject to parametric uncertainties without coordinate partitioning. This was possible through judicious design of extended error, that is based on the orthogonalization principle. Afterwards, several schemes have been proposed based on the orthogonalization principle, however these schemes have not been extended or combined beyond constrained robots.

III. NONLINEAR ROBOT DYNAMICS

A. Constrained robot dynamics

The constrained robot dynamics arises when its end effector is in contact to infinitely rigid surface. Considering the generalized position² $q \in \mathbb{R}^n$ and velocity coordinates $\dot{q} \in \mathbb{R}^n$, this system can be modeled as a set of differential algebraic equation as follows [6]

$$\begin{aligned} H(q)\ddot{q} + C(q, \dot{q})\dot{q} + g(q) &= \tau + J_{\varphi+}^T(q)\lambda - F(\dot{q}, \dot{z}, z) \quad (1) \\ \varphi(q) &= 0 \quad (2) \end{aligned}$$

where matrix $H(q) \in \mathbb{R}^{n \times n}$ stands for the symmetric positive definite manipulator inertia matrix; $C(q, \dot{q})\dot{q} \in \mathbb{R}^n$ stands for the vector of centripetal and Coriolis torques; $g(q) \in \mathbb{R}^n$ is

²No independent reduction of generalized coordinates was used in this approach.

the vector of gravitational torques, $F(\dot{q}, \dot{z}, z)$ is the dynamic friction³, $J_{\varphi+}(q) = \frac{J_{\varphi}}{J_{\varphi} J_{\varphi}^T}$ is the constrained normalized jacobian of the the kinematic constraint $\varphi(q) = 0$ or rigid surface assumed frictionless with continuous gradient and λ stands for the constrained lagrangian, or contact force. Adding and subtracting to (1)-(2) the following linear parametrization arises

$$H(q)\ddot{q}_r + C(q, \dot{q})\dot{q}_r + g(q) = y_r \theta_b \quad (3)$$

where the known regressor $y_r = y_r(q, \dot{q}, \ddot{q}_r) \in \mathbb{R}^{m \times p}$ and the unknown constant vector $\theta_b \in \mathbb{R}^p, p > 0$, produces the open loop error equation

$$H(q)\dot{S}_q = \tau + J_{\varphi+}^T(q)\lambda - C(q, \dot{q})S_q - y_r \theta_b \quad (4)$$

with joint error surface S_q defined as

$$S_q = \dot{q} - \dot{q}_r \quad (5)$$

where \dot{q}_r stands for the nominal reference of joint velocities, not yet defined.

IV. CAMERA MODEL

The static pin hole camera model is used, considering thin lens without aberration [7]. To introduce the model, first consider the robot direct kinematics

$$x_b = f(q) \quad (6)$$

where $x_b \in \mathbb{R}^n$ represents the position of robot end effector in cartesian space, $q \in \mathbb{R}^n$ is the vector of generalized joint displacements, and $f(\cdot) : \mathbb{R}^n \rightarrow \mathbb{R}^n$. Then, the differential kinematics of robot manipulator, which relates velocities in cartesian space $\dot{x}_b \in \mathbb{R}^n$ to joint space velocities $\dot{q} \in \mathbb{R}^n$, is defined as follows

$$\dot{x}_b = J(q)\dot{q} \quad (7)$$

Now, the visual position $x_s \in \mathbb{R}^2$ of robot end effector in monochromatic image space (screen) is given by [7]

$$x_s = \alpha R(\theta) x_b + \beta_s \quad (8)$$

where α is the scale factor⁴, and $R(\theta) \in SO(3)$, $\beta_s \in \mathbb{R}^2$ and depends on intrinsic and extrinsic parameters of camera⁵. The differential camera model is then

$$\dot{x}_s = \alpha R(\theta) \dot{x}_b \quad (9)$$

where $\dot{x}_s \in \mathbb{R}^2$ determines the visual robot end effector velocity. Notice that the constant transformation $\alpha R(\theta)$ maps statically *robot* cartesian velocities \dot{x}_b into *visual* velocities or *visual flow* \dot{x}_s .

Using equation (6)~(8), equation (9) becomes

$$\dot{x}_s = \alpha R(\theta) J(q)\dot{q} \quad (10)$$

³For a clear exposition, firstly, $F(\dot{q}, \dot{z}, z)$ will be considered zero, however in Section VIII it will be treated.

⁴Without loss of generality, α can be considered as a scalar matrix 2×2 .

⁵Focal distance, depth of field, translation of camera center to image center, distance between optical axe and the robot base.

Thus, the inverse differential kinematics for robot manipulator in terms of visual velocities⁶ becomes

$$\dot{q} = J(q)^{-1} R(\theta)^{-1} \alpha^{-1} \dot{x}_s \Rightarrow \dot{q} = J_{Rinv} \dot{x}_s \quad (11)$$

This relation is useful to design the nominal reference of joint velocities \dot{q}_r in the following section.

V. VISUAL ORTHOGONALIZATION PRINCIPLE

Since $\varphi(q) = 0 \forall t$, then its time derivative yields

$$\frac{d}{dt} \varphi(q) = \frac{\partial \varphi(q)}{\partial q} \frac{dq}{dt} \equiv J_\varphi(q) \dot{q} = 0$$

This means that $J_\varphi(q)$ is orthogonal to \dot{q} . That is, \dot{q} belongs to the orthogonal projection matrix Q of $J_\varphi(q)$ [6]

$$Q = I - J_{\varphi+}^T J_\varphi \quad (12)$$

As we can see, Q spans the tangent plane at the contact point, therefore, J_φ and Q are orthogonal complements. In other words, *if the robot end effector is in contact with the constraint surface*, then

$$Q\dot{q} = \dot{q} \rightarrow QQ\dot{q} = Q\dot{q} \equiv \dot{q} \quad (13)$$

that is, Q is idempotent; therefore naturally,

$$QJ_\varphi^T = 0 \quad (14)$$

These properties are fundamental to establish the *visual orthogonalization principle* as follows. Firstly consider \dot{q}_r in terms of orthogonal nominal references of velocity \dot{q}_s and force \dot{q}_f , as follows

$$\dot{q}_r = \dot{q}_s + \dot{q}_f \quad (15)$$

Notice that, we are also interested in designing an image based servo visual force control without computing inverse kinematics⁷, then nominal reference \dot{q}_r must be designed in terms of nominal visual reference and nominal force reference as follows

$$\dot{q}_r = QJ_{Rinv} \dot{x}_r + \beta J_\varphi^T \dot{q}_{rf} \quad (16)$$

with $\dot{q}_s = QJ_{Rinv} \dot{x}_r$ and $\dot{q}_f = \beta J_\varphi^T \dot{q}_{rf}$, $\beta \in \mathbb{R}_+$.

Using (11) and (13), consider now the next *nominal visual reference* of velocities

$$\dot{x}_r = \dot{x}_{sd} - \alpha \Delta x_s + S_{sd} - \gamma_{s1} \int_{t_0}^t S_{s\delta} - \gamma_{s2} \int_{t_0}^t \text{sign}(S_{s\delta}) \quad (17)$$

where \dot{x}_{sd} stands for desired visual velocity trajectory, and $\Delta x_s = x_s - x_{sd}$ is the visual position error. Finally, the visual error surface arises

$$S_{s\delta} = S_s - S_{sd} \equiv (\Delta \dot{x}_s + \alpha \Delta x_s) - S_s(t_0) e^{-\kappa_s t} \quad (18)$$

where $\Delta \dot{x}_s = \dot{x}_s - \dot{x}_{sd}$ defines visual velocity error, $\kappa_s > 0$ and $\gamma_{si} = \gamma_{si}^T \in \mathbb{R}_+^{n \times n}$, $i = 1, 2$.

⁶With $J_{Rinv} \in \mathbb{R}^{n \times n}$ whose entries are functions of robot and camera parameters.

⁷to eliminate the inverse kinematics calculus and to reduce the control law computational cost. This is also one byproduct of this scheme.

Now, let consider now the *nominal force reference* as

$$\dot{q}_{rf} = \Delta F - S_{dF} + \gamma_{F1} \int_{t_0}^t S_{F\delta} + \gamma_{F2} \int_{t_0}^t \text{sign}(S_{F\delta}) \quad (19)$$

for

$$S_{F\delta} = S_F - S_{Fd} \equiv \Delta F - S_F(t_0) e^{-\kappa_F t} \quad (20)$$

where $\Delta F = \int_{t_0}^t \Delta \lambda(\zeta) d\zeta$, $\Delta \lambda = \lambda - \lambda_d$, λ_d is the desired contact force, $\kappa_F > 0$, and $\gamma_{Fi} = \gamma_{Fi} \in \mathbb{R}_+^{n \times n}$, $i = 1, 2$.

Using equations (16), (17), (19) and (11) into (5), the visual orthogonalized joint error surface arise as follows

$$\begin{aligned} S_q &= \dot{q} - \dot{q}_r \equiv Q\dot{q} - \dot{q}_r \\ &= QJ_{Rinv} \dot{x}_s - QJ_{Rinv} \dot{x}_r - \beta J_\varphi^T \dot{q}_{rf} \\ &= QJ_{Rinv} S_{vs} - \beta J_\varphi^T S_{vF} \end{aligned} \quad (21)$$

with

$$\begin{aligned} S_{vs} &= S_{s\delta} + \gamma_{s1} \int_{t_0}^t S_{s\delta} + \gamma_{s2} \int_{t_0}^t \text{sign}(S_{s\delta}) \\ S_{vF} &= S_{F\delta} + \gamma_{F1} \int_{t_0}^t S_{F\delta} + \gamma_{F2} \int_{t_0}^t \text{sign}(S_{F\delta}) \end{aligned}$$

where S_{vs} stands for the visual manifold and S_{vF} stands for the force manifold.

Notice that S_q is composed of two orthogonal complements $QJ_{Rinv} S_{vs}$ depending on image coordinate error, and $\beta J_\varphi^T S_{vF}$ depending of integral of contact force errors. Thus, tracking errors Δx_s and ΔF can be controlled independently, since they are mapped to orthogonal complements.

Remark 1. The above definition assumes exact knowledge of J_{Rinv} . However, in practice, it stands as a very restricted assumption. Therefore, we need to design a uncertain manifold S_q taking into consideration the uncertainty of J_{Rinv} . To this end, consider

$$\widehat{\dot{q}}_r = Q\widehat{J_{Rinv}} \dot{x}_r + \beta J_\varphi^T \dot{q}_{rf} \quad (22)$$

with $\widehat{J_{Rinv}}$ an estimated of J_{Rinv} , such that $\text{rank}(\widehat{J_{Rinv}})$ are full rank $\forall q \in \Omega$, where the robot workspace free of singularities is defined by $\Omega = \{q | \text{rank}(J(q)) = n, \forall q \in \mathbb{R}^n\}$, and $\forall \theta \in \mathbb{R}$. Thus, substituting (22) into (5), we have the *uncalibrated joint error surface*

$$\begin{aligned} \widehat{S}_q &= \dot{q} - \widehat{\dot{q}}_r \\ &= QJ_{Rinv} \dot{x}_s - Q\widehat{J_{Rinv}} \dot{x}_r - \beta J_\varphi^T \dot{q}_{rf} \end{aligned} \quad (23)$$

where \widehat{S}_q is available because \dot{q} and $\widehat{\dot{q}}_r$ are available. Adding and subtracting $QJ_{Rinv} \dot{x}_r$ to (23) we obtain

$$\begin{aligned} \widehat{S}_q &= QJ_{Rinv} S_{vs} - \beta J_\varphi^T S_{vF} - Q\Delta J_{Rinv} \dot{x}_r \\ &= S_q - Q\Delta J_{Rinv} \dot{x}_r \end{aligned} \quad (24)$$

where $\Delta J_{Rinv} = \widehat{J_{Rinv}} - J_{Rinv}$.

Remark 2. *Uncalibrated visual system.* In this paper we regarded an uncalibrated visual scheme, i.e., J_{Rinv} is considered as unknown. This means that the complete product of J_{Rinv} is unknown even when $J(q)$ is known, since J_φ and Q are known.

VI. OPEN LOOP ERROR EQUATION

Using (22), the uncertain parametrization $y_r \hat{\theta}_b$ becomes

$$H(q)\hat{q}_r + C(q, \dot{q})\hat{q}_r + g(q) = y_r \hat{\theta}_b \quad (25)$$

where $\hat{q}_r = f(\ddot{x}_r, \ddot{q}_{fr})$, with

$$\ddot{x}_r = \ddot{x}_{sd} - \alpha \Delta \dot{x}_s + \dot{S}_{sd} - \gamma_{s1} S_{s\delta} - \gamma_{s2} \text{sign}(S_{s\delta}) \quad (26)$$

$$\ddot{q}_{rf} = \Delta \dot{F} - \dot{S}_{dF} + \gamma_{F1} S_{F\delta} + \gamma_{F2} \text{sign}(S_{F\delta}) \quad (27)$$

which introduces discontinuous terms. To avoid introducing high frequency discontinuous signals, add and subtract $\tanh(v_s S_{s\delta})$ and $\tanh(v_f S_{F\delta})$, $v_f, v_s > 0$, to \hat{q}_r to separate continuous and discontinuous signals as follows

$$\hat{q}_r = \hat{q}_{rcont} + Q\gamma_s z_s - \beta J_\varphi^T \gamma_f z_f \quad (28)$$

with $z_s = \tanh(\lambda_s S_{s\delta}) - \text{sign}(S_{s\delta})$ and $z_f = \tanh(\lambda_f S_{F\delta}) - \text{sign}(S_{F\delta})$. Thus $y_{rcont} = y_r(q, \dot{q}, \hat{q}_r, \hat{q}_{rcont})$ is continuous since $(\hat{q}_r, \hat{q}_{rcont}) \in C^1$, where

$$\hat{q}_{rcont} = Q\widehat{J_{Rinv}}\ddot{x}_{rcont} + \dot{Q}\widehat{J_{Rinv}}\dot{x}_{rcont} + Q\widehat{J_{Rinv}}\dot{x}_{rcont} + \beta J_\varphi^T \ddot{q}_{rfcont} + \beta J_\varphi^T \dot{q}_{rfcont} \quad (29)$$

with

$$\ddot{x}_{rcont} = \ddot{x}_{sd} - \alpha \Delta \dot{x}_s + \dot{S}_{sd} - \gamma_{s1} S_{s\delta} - \gamma_{s2} \tanh(v_s S_{s\delta}) \quad (30)$$

$$\ddot{q}_{rfcont} = \Delta \dot{F} - \dot{S}_{dF} + \gamma_{F1} S_{F\delta} + \gamma_{F2} \tanh(v_f S_{F\delta}) \quad (31)$$

Therefore (25) becomes

$$H(q)\hat{q}_r + C(q, \dot{q})\hat{q}_r + g(q) = y_{rcont} \hat{\theta}_b + H(Q\gamma_s z_s - \beta J_\varphi^T \gamma_f z_f) \quad (32)$$

Adding and subtracting (32) to (1), we obtain finally the open loop error in function of $(q, \dot{q}, \hat{q}_r, \hat{q}_{rcont})$ as follows:

$$H(q)\hat{S}_q = \tau - C(q, \dot{q})\hat{S}_q + J_{\varphi+}^T(q)\lambda - y_{rcont} \hat{\theta}_b + H(Q\gamma_s z_s - \beta J_\varphi^T \gamma_f z_f) \quad (33)$$

Now we are ready to present the main result.

VII. CONTROL DESIGN

Theorem 1 Assume that initial conditions and desired trajectories belong to Ω , and consider the robot dynamics (1) in closed loop with the following visual adaptive force-position control law

$$\tau = -K_d \hat{S}_q + y_{rcont} \hat{\theta}_b + J_{\varphi+}^T(q) [-\lambda_d + \eta \Delta F] + \gamma_F J_\varphi^T(q) * \left[\tanh(v_F S_{F\delta}) + \eta \int_{t_0}^t \text{sgn}(S_{F\delta}) \right] \quad (34)$$

$$\dot{\hat{\theta}}_b = -\Gamma y_{rcont}^T \hat{S}_q \quad (35)$$

where $\Gamma \in \mathfrak{R}_+^{p \times p}$, $K_d \in \mathfrak{R}_+^{n \times n}$, $\eta > 0$. If K_d is large enough and error of initial conditions are small enough, and if

$$\gamma_s \geq \left\| \frac{d}{dt} \left\{ R_\alpha(\theta) J(q) \left[\hat{S}_q + (\Delta J_{Rinv}) \dot{x}_r \right] \right\} \right\|$$

$$\gamma_F \geq \left\| \frac{d}{dt} \left[(J_\varphi J_\varphi^T(q))^{-1} J_\varphi \hat{S}_q \right] \right\|$$

then exponential convergence of visual and force tracking errors is guaranteed.

Proof: The proof can be found in the appendix.

Remark 3. Apparently there is problem with $J(q(t))^{-1}$. However, we have proved that $J(q(t))$ is not singular for all time, because $q(t) \rightarrow q_d(t)$ exponentially, without overshoot, with desired trajectories belonging to robot workspace Ω , thus $J(q(t)) \rightarrow J(q_d(t))$ within Ω and $J(q(t))^{-1}$ is well-posed $\forall t$.

Remark 4. Since the continuous $\tanh(*)$ is substituted instead of $\text{sign}(*)$, upper bounds ε_2 and ε_3 are greater. To induce the second order sliding mode, and therefore exponential convergence of tracking errors, it suffices to tune γ_{s2} and γ_{F2} to a larger value. If $\text{sign}(*)$ would have been used, then smaller γ_{s2} and γ_{F2} would have been tuned, but at the price of chattering on the control input.

Remark 5. In this article, a new control law has been proposed, which is easy to implement and presents low computational cost, even when the proof is quite involved to follow, however, straightforward.

VIII. DYNAMIC FRICTION COMPENSATION

The following *LuGre* [8] dynamic friction model is considered

$$\begin{aligned} F(\dot{q}, \dot{z}, z) &= \sigma_0 z + \sigma_1 \dot{z} + \sigma_2 \dot{q} \\ \dot{z} &= -\sigma_0 h(\dot{q}) z + \dot{q} \\ h(\dot{q}) &= \frac{|\dot{q}|}{\alpha_0 + \alpha_1 \exp^{-(\dot{q}/\dot{q}_s)^2}} \end{aligned} \quad (36)$$

where matrix parameters $\sigma_1, \sigma_2, \sigma_3$ are diagonal definite matrices $n \times n$, the state $z \in \mathfrak{R}^n$ stands for the position of the bristles, $\alpha_0, \alpha_1 > 0$, and $\dot{q}_s > 0$. We just want to highlight that this model exhibits the following complex dynamic friction effects (see [8] for more details on this model).

- Backlash.
- Viscous friction.
- Stiction and static friction.
- Stribeck effect.
- Elastic and plastic deformation.
- Pre-sliding regime.

These effects involve a very complex dynamics around the trivial equilibrium, and for bidirectional motion, and for very small displacements, the forces that comes out from this model makes impossible to reach the origin due to the limit cycles induced and the potentially unstable behavior.

Substituting (36) into (1) yields

$$H(q)\ddot{q} + C(q, \dot{q})\dot{q} + \sigma_{12}\dot{q} + g(q) + \sigma_0 z - \sigma_{01} h(\dot{q}) z = \tau + J_{\varphi+}^T(q)\lambda \quad (37)$$

where $\sigma_{01} = \sigma_0 \sigma_1$ and $\sigma_{12} = \sigma_1 + \sigma_2$. Substituting the uncalibrated nominal reference (22) in (37), just like (25), lies the next equation

$$H(q)\hat{q} + C(q, \dot{q})\hat{q} + \sigma_{12}\hat{q} + g(q) + \sigma_0 z - \sigma_{01} \hat{h}(\dot{q}) z = \tau + J_{\varphi+}^T(q)\lambda \quad (38)$$

Similar to [9], only the part of the equation (38) that is linear in parameters (LP) is rewritten in terms of the

uncalibrated nominal reference $(\hat{q}_r, \hat{\dot{q}}_r)^T \in \mathbb{R}^{2n}$ as follows

$$H(q)\hat{\dot{q}}_r + C(q, \dot{q})\hat{q}_r + \sigma_{12}\hat{\dot{q}}_r + g(q) = Y_r\hat{\Theta}_b + \sigma_{12}\hat{\dot{q}}_r \quad (39)$$

Notice that $y_r\hat{\theta}_b \neq Y_r\hat{\Theta}_b$. To be able to cast the problem of non-LP of equation (36) as a disturbance rejection problem, [9] proposes a discontinuous virtual regressor, which in turn yields chattering, with harmful consequences to real physical systems. To avoid chattering the following virtual *continuous* regressor is introduced

$$\frac{\sigma_{01}\alpha_{01}}{\alpha_0}|\dot{q}|\tanh(\xi_f\hat{S}_q) + \sigma_0\alpha_{01}\tanh(\xi_f\hat{S}_q) = Y_f\Theta_f, \quad (40)$$

where $\alpha_{01} = \alpha_0 + \alpha_1$, $\tanh(q)$ is the continuous hyperbolic tangent function, and $\lambda_f > 0$. If we add and subtract (39) and (40) to (37), the following parametrization arises

$$H(q)\hat{S}_q + C(q, \dot{q})\hat{S}_q + \sigma_{12}\hat{S}_q = \tau - \mathcal{F} - Y\hat{\Theta} + J_{\varphi+}^T(q)f \quad (41)$$

with

$$\begin{aligned} \mathcal{F} = \sigma_0 \left\{ z + \alpha_{01}\tanh(\xi_f\hat{S}_q) \right. \\ \left. + \alpha_0^{-1}\sigma_1\alpha_{01}|\dot{q}|\tanh(\xi_f\hat{S}_q) \right. \\ \left. - \sigma_1|\dot{q}|z(\alpha_0 + \alpha_1\exp^{-(\dot{q}/\dot{q}_s)^2})^{-1} \right\} \end{aligned} \quad (42)$$

where $Y = [Y_r, Y_f]$, and $\hat{\Theta} = [\hat{\Theta}_b^T, \Theta_f^T]^T$. Finally, solving (41) for $H(q)\hat{S}_q$, yields the following open-loop visual error dynamics subject to dynamic friction

$$H(q)\hat{S}_q = -C(q, \dot{q})\hat{S}_q - \sigma_{12}\hat{S}_q + \tau - \mathcal{F} - Y\hat{\Theta} + J_{\varphi+}^T(q)f \quad (43)$$

Finally, consider the following visual adaptive force-position control law

$$\begin{aligned} \tau = -K_d\hat{S}_q + Y\hat{\Theta} + J_{\varphi+}^T(q)[- \lambda_d + \eta\Delta F] + \\ \gamma_F J_{\varphi+}^T(q) * \left[\tanh(\mu S_{F\delta}) + \eta \int_{t_0}^t \text{sgn}(S_{F\delta}) \right] \end{aligned} \quad (44)$$

$$\hat{\Theta} = -\Gamma Y^T \hat{S}_q \quad (45)$$

where $\Gamma \in \mathbb{R}^{p \times p+}$, $K_d \in \mathbb{R}_+^{n \times n}$. We now have the following result.

Theorem 2 Assume that initial conditions and desired trajectories belong to Ω , and consider the controller (44)-(45). If K_d is large enough and a error of initial conditions are small enough, and if

$$\begin{aligned} \gamma_s \geq \left\| \frac{d}{dt} \left\{ R_\alpha(\theta) J(q) \left[\hat{S}_q + \Delta J_{Rinv} \dot{x}_r \right] \right\} \right\| \\ \gamma_F \geq \left\| \frac{d}{dt} \left[(-\beta J_\varphi J_\varphi^T(q))^{-1} J_\varphi \hat{S}_q \right] \right\| \end{aligned}$$

then exponential convergence of visual and force tracking errors is guaranteed.

Proof: The proof can be found in the appendix.

Remark 6. *Important properties of this control scheme have to be highlighted: Is an Image-based dynamical control*

scheme for constrained robots that fuses visual, encoder and force signals. This control law presents, for first time in literature, compensation of dynamic friction by means of visual feedback.

IX. SIMULATIONS

The simulations were carry out in Matlab Simulink software. Robot parameters and constant gains used in the simulations are: $(m_1, m_2) = (6.72, 2.03) Kg$, $(l_1, l_2) = (0.4, 0.3) m$. The desired trajectories for the simulation was: $x_s = \alpha R[xcd; ycd] + \beta_s$, $xcd = 0.5$; $ycd = 0.5 + r * \sin(\omega * t)$; $r = 0.1$, $\omega = 0.5$. The contact surface (restriction) is a plane parallel to plane YZ and over $x = 0.5$;

In order to simulate a non calibrated system, we used 20% of uncertainty in each element of J_{Rinv} , this rise a 50% of J_{Rinv} uncertainty. The constant values for the simulation are: $\Gamma = 1$, $\kappa_f = 20$, $\gamma_f = 3.0$, $\eta = 0.029$, $\beta = 1.0$, $K_d = 90$, $\alpha = 40$, $\kappa_s = 20$, $\gamma_s = 7.8$. Friction parameters: $\sigma_0 = 30000$, $\sigma_{1,2} = 2$, $\alpha_{0,1} = (4, 0.4)$, $\dot{q}_s = 0.01$. Figures (2) and (3) depict the cartesian and visual error, respectively. Figure (4) shows the contact force applied on the wall. Figure (5) renders the smooth and chattering-free input control for each link. Finally, in Figure (6) can be seen the 3D task space. Notice the difference between compensation and not compensation of dynamic friction in each figure. The control laws described above were quite easy to tune and present minimum errors of visual and force tracking without high frequencies in the control input.

X. CONCLUSIONS

This paper introduces a novel scheme for adaptive image based visual servoing/force control in a constrained dynamical system. The main feature is the ability to fuse image coordinates into a orthogonal complement of joint velocities, and contact forces in the orthogonal complement of integral of contact forces. Using this, exponential convergence arises for image-based position-velocity and contact forces even when robot parameters and camera parameters are considered unknown. Additionally, it is proposed a compensator of uncertain dynamic friction, which is usually neglected in visual servoing, but it is of particularly concern in visual motion tasks, because the motion regime is slow, with velocity reversals. Simulations confirm the predicted stability properties.

ACKNOWLEDGEMENTS

E. Dean and L. Garcia thank CONACYT support under a doctoral scholarship #158973 and #158613. V. Parra-Vega carries out this research while he is on a sabbatical leave from Mechatronics Division, CINVESTAV, at the Information Technology Division of CIATEQ. This author acknowledges support from CONACYT project number 39727-Y.

REFERENCES

- [1] A. Namiki, Y. Nakabo, I. I. M. I., High speed grasping using visual and force feedback. Proceedings of the 1999 IEEE International Conference on Robotics and Automation, Detroit, MI, pages 3195–3200.

- [2] B. Nelson, P. (October, 1996), Force and vision resolvability for assimilating disparate sensory feedback, *IEEE Trans. on Robot. and Autom.* 1996, 12(5):714–731.
- [3] J. Baeten, W. Verdonck, H. B. J. D. S., Combining force control and visual servoing for planar contour following. *Machine Intelligence and Robotic Control*. 2000, 2(2):69–75.
- [4] S. Jorg, J. Langwald, J. S. G. H. C. N., Flexible robot assembly using a multi-sensory approach, *Proc. of the 2000 IEEE Int. Conf. Robot. and Autom.*, San Francisco, CA, pages 3687–3694.
- [5] Xiao, D., Sensor-hybrid Position/Force control of a robot manipulator in an uncalibrated environment, *IEEE Trans. Control System Technology*, 2000, 8(4):635–645.
- [6] S. Arimoto, Y. H. Liu and T. Naniwa, Model Based Adaptive Hybrid Control for Geometrically Constrained Robot Manipulator, *Proc. IEEE Int. Conf. on Rob. and Autom.* 1996, pp. 618-623.
- [7] S. Hutchinson, G. Hager, P. C., A tutorial on visual servo control, *Trans. on Robotics and Automation*. 1996. Vol. 6, 651-670
- [8] Canudas de Wit, C., Olsson, H., and Astrom, K.J., "A New Model for Control of Systems with Friction," *IEEE Transactions of Automatic Control*, 1995, Vol. 40., No. 3, 419-425.
- [9] Panteley, E., Ortega, R., & Gafvert, M., An Adaptive Friction Compensator for Global Tracking in Robot Manipulators, *Systems and Control Letters*, 1998, Vol. 33, No. 5, 307 - 313.
- [10] V. Parra-Vega, S. Arimoto, Y. L. G. H. P. A., Dynamic sliding PID control for tracking of robot manipulators: Theory and experiments, *IEEE Transactions on Robotics and Automation*. 2003. Vol. 19., 967-976.
- [11] Parra-Vega, V., Adaptive compensation of dynamic friction in finite time of 1 DOF mechanical system. *American Control Conference*, 2001. Proceedings of the 2001, Volume: 3, 25-27 June 2001, pp: 2462 - 2467 vol.3
- [12] García-Valdovinos, L. G., Seguimiento Perfecto en Tiempo Finito de Robots Manipuladores Sujetos a Fricción Dinámica, Master Thesis, Dept of EE, Mechatronics Division, CINVESTAV-IPN, México, D.F., 2003.
- [13] Parra-Vega, V., García-Rodríguez, R., Dean-León, E., and Ruiz-Sanchez, F., And Adaptive Neural Network Controller for Visual Tracking of Constrained Robot Manipulators, *American Control Conference (ACC 2005)*, June 8-10, 2005, Portland, Oregon.

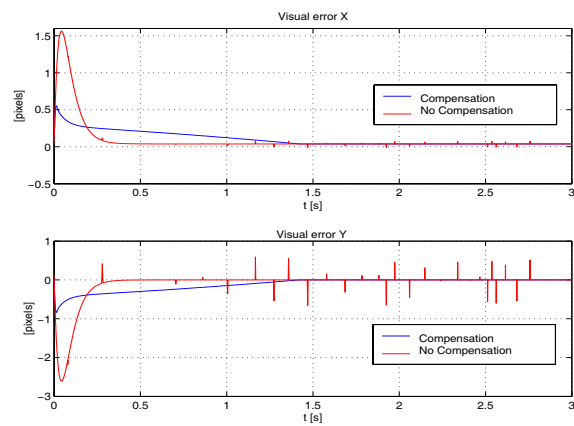


Fig. 3. Visual tracking error with exponential envelope.

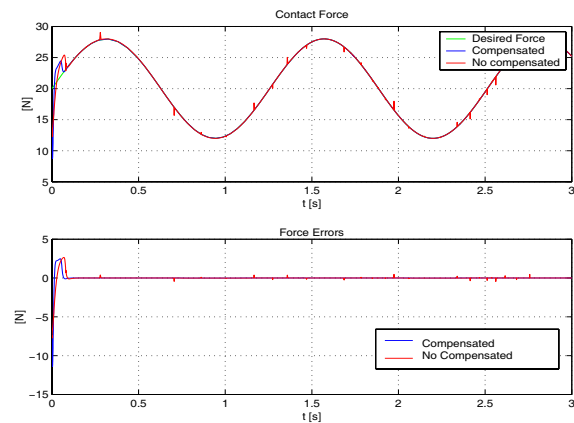


Fig. 4. Force tracking errors indicate very fast convergence with short transient due to the adapted unknown parameters.

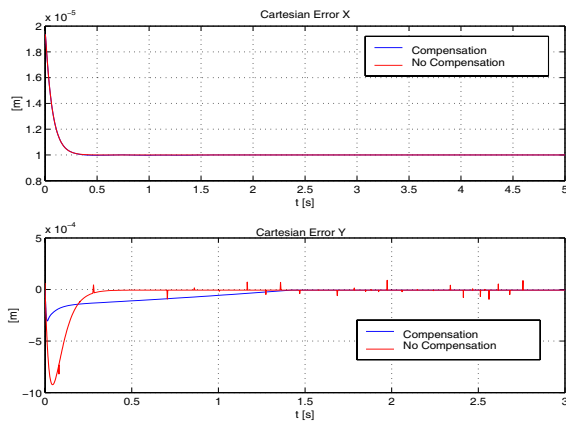


Fig. 2. Cartesian tracking error with exponential envelope.

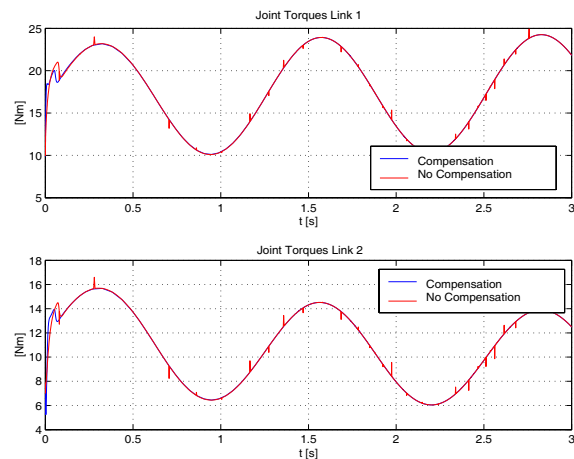


Fig. 5. Control input with very smooth activity.

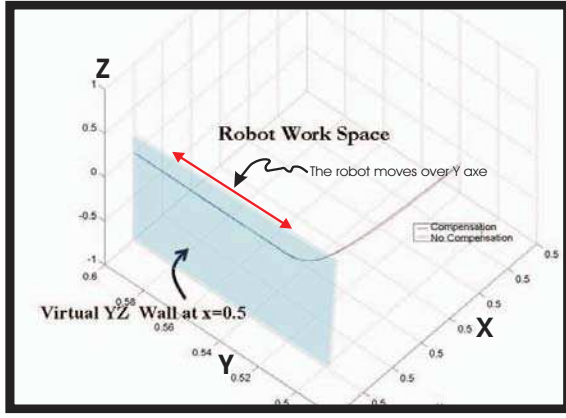


Fig. 6. 3D view of the task cartesian space.

APPENDIX

Theorem 1 : Proof. The closed loop dynamics between (34)~(35) and (33) yields

$$H(q)\hat{S}_q = -\{K_d + C(q, \dot{q})\}\hat{S}_q - y_{cont}\Delta\theta_b + J_{\varphi+}^T(q)[\Delta\lambda + \gamma_F \tanh(\mu S_{F\delta})] + \eta J_{\varphi+}^T(q) \left[\Delta F + \gamma_F \int \text{sgn}(S_{F\delta}) \right] \quad (46)$$

$$\Delta\dot{\theta}_b = \Gamma y_{cont}^T \hat{S}_q \quad (47)$$

with $\Delta\theta_b = \theta_b - \hat{\theta}_b$. The proof is organized in three parts.

Part I. Boundedness of Closed Loop Trajectories. Consider the time derivative of the following *Lyapunov* candidate function

$$V = \frac{1}{2} \left[\hat{S}_q^T H(q) \hat{S}_q + \beta S_{vF}^T S_{vF} + \Delta\theta_b^T \Gamma^{-1} \Delta\theta_b \right] \quad (48)$$

along the solutions of (46)-(47) as

$$\dot{V} \leq -K_d \left\| \hat{S}_q \right\|_2^2 - \eta\beta \|S_{vF}\| + \|\hat{S}_q\| \psi \quad (49)$$

where ψ is a functional depending on the state and error manifolds, similarly to [10]. Now if K_d , η and β are large enough and the initial errors are small enough, we conclude the seminegative definiteness of (49) outside of hyperball $\varepsilon_0 = \left\{ \hat{S}_q | \dot{V} \leq 0 \right\}$ centered at the origin, such as the following properties of the state of closed loop system arise

$$\hat{S}_q, S_{vF} \in \mathcal{L}_\infty \rightarrow \|S_{vs}\|, \|S_{vF}\| \in \mathcal{L}_\infty \quad (50)$$

Then, $(S_{s\delta}, \int \text{sgn}(S_{s\delta})) \in \mathcal{L}_\infty$, and since desired trajectories are C^2 and feedback gains are bounded, we have that $(\hat{q}_r, \dot{\hat{q}}_r) \in \mathcal{L}_\infty$. The right hand side of (33) shows that $\varepsilon_1 > 0$ exists such that

$$\left\| \hat{S}_q \right\| \leq \varepsilon_1$$

This result shows only local stability of \hat{S}_q and $\dot{\hat{S}}_q$. Now we prove that the sliding modes arises.

Rewriting (24) in terms of two orthogonal vectors, we obtain

$$\dot{\hat{S}}_q = Q \{ J_{Rinv} S_{vs} - \Delta J_{Rinv} \dot{x}_r \} - \beta J_{\varphi}^T \{ S_{vF} \} \quad (51)$$

Since $\hat{S}_q \in \mathcal{L}_2$, and J_{Rinv} and Q are bounded, then $Q J_{Rinv} S_{vs}$ is bounded and, due to $\varphi(q)$ is smooth and lies in the reachable robot space and $S_{vF} \rightarrow 0$, then $\beta J_{\varphi}^T S_{vF} \rightarrow 0$. Now, taking into account that $\dot{\hat{S}}_q$ is bounded, then $\frac{d}{dt} J_{Rinv} Q S_{vs}$ and $\frac{d}{dt} \beta J_{\varphi}^T S_{vF}$ are bounded (this is possible because J_{φ}^T is bounded and so \dot{Q} is). All this chains of conclusions proves that there exists constants $\varepsilon_2 > 0$ and $\varepsilon_3 > 0$ such that

$$\left| \dot{S}_{vs} \right| < \varepsilon_2, \left| \dot{S}_{vF} \right| < \varepsilon_3$$

Now, we have to prove that for a proper selection of feedback gains γ_{s1} , γ_{s2} and γ_{F1} , γ_{F2} then trajectories of visual position and force converges to zero. This is possible if we can prove that sliding modes are established in the visual position subspace Q and in the subspace of force $J_{\varphi}^T(q)$. Considering that operator $Q J_{Rinv}$ spans the vector \hat{S}_q as the direct sum of its image $im \{ Q J_{Rinv} (S_{vs}) \} \equiv S_{vs}^{im}$ and $im \{ \beta J_{\varphi}^T (S_{vF}) \} \equiv S_{vF}^{im}$, see (51), this implies that

$$\begin{aligned} \hat{S}_q &= Q \{ J_{Rinv} S_{vs} - \Delta J_{Rinv} \dot{x}_r \} - \beta J_{\varphi}^T \{ S_{vF} \} \\ &= (S_{vs}^{im} - im \{ \Delta J_{Rinv} \dot{x}_r \}) - S_{vF}^{im} \end{aligned} \quad (52)$$

where $S_{vs}^{im} - im \{ \Delta J_{Rinv} \dot{x}_r \}$ and S_{vF}^{im} belongs to orthogonal complements, that means $\langle S_{vs}^{im} - im \{ \Delta J_{Rinv} \dot{x}_r \}, S_{vF}^{im} \rangle = 0$. That is, we are able to analyze the $S_{vs}^{im} - im \{ \Delta J_{Rinv} \dot{x}_r \}$ dynamics independently of S_{vF}^{im} , because S_{vF}^{im} belongs to the kernel of Q . This is verified if we multiply (52) by Q^T , that is

$$\begin{aligned} Q^T \hat{S}_q &= Q^T Q \{ J_{Rinv} S_{vs} - \Delta J_{Rinv} \dot{x}_r \} - \beta Q^T J_{\varphi}^T S_{vF} \\ &= S_{vs}^{im} - im \{ \Delta J_{Rinv} \dot{x}_r \} \end{aligned} \quad (53)$$

since Q is idempotent. It is important to notice that if $Ax = Ay$ for any square nonsingular matrix A and any couple of vectors x, y , then $x \equiv y$. Thus, equation (53) means that $\hat{S}_q = Q \{ J_{Rinv} S_{vs} - \Delta J_{Rinv} \dot{x}_r \}$ is valid within span of Q . Now, if we multiply \hat{S}_q by $J_{\varphi+}$ we obtain

$$\begin{aligned} J_{\varphi+} \hat{S}_q &= J_{\varphi+} Q \{ J_{Rinv} S_{vs} - \Delta J_{Rinv} \dot{x}_r \} - \beta J_{\varphi+} J_{\varphi}^T \{ S_{vF} \} \\ &= -\beta S_{vF} \end{aligned} \quad (54)$$

Part II: Second Order Sliding Modes.

Part II.a: Sliding modes for the velocity subspace.

According to $Q^T \hat{S}_q = Q \{ J_{Rinv} S_{vs} - \Delta J_{Rinv} \dot{x}_r \}$ then $\hat{S}_q \equiv J_{Rinv} S_{vs} - \Delta J_{Rinv} \dot{x}_r$ in the image subspace of Q , however notice that Q is not full rank, then this equivalence is valid locally, not globally. In this local neighborhood, if we multiply $\hat{S}_q = Q \{ J_{Rinv} S_{vs} - \Delta J_{Rinv} \dot{x}_r \}$ by $R_\alpha(\theta) J(q)^8$,

⁸Remember the equality: $J_{Rinv} = J^{-1}(q) R_\alpha^{-1}(\theta)$.

we have

$$R_\alpha(\theta) J(q) \hat{S}_q = S_{s\delta} + \gamma_{s1} \int_{t_0}^t S_{s\delta} + \gamma_{s2} \int_{t_0}^t \text{sign}(S_{s\delta}) - R_\alpha(\theta) J(q) \{\Delta J_{Rinv} \dot{x}_r\} \quad (55)$$

Taking the time derivative of (55), and multiply it by $S_{s\delta}^T$ produces

$$\begin{aligned} S_{s\delta}^T \dot{S}_{s\delta} &= -\gamma_{s2} S_{s\delta}^T \text{sign}(S_{s\delta}) - \gamma_{s1} S_{s\delta}^T S_{s\delta} + \\ & S_{s\delta}^T \frac{d}{dt} \left[R_\alpha(\theta) J(q) \left(\hat{S}_q + \Delta J_{Rinv} \dot{x}_r \right) \right] \\ &\leq -\mu_s |S_{s\delta}| - \gamma_{s1} \|S_{s\delta}\|^2 \end{aligned} \quad (56)$$

where $\mu_s = \gamma_{s1} - \varepsilon_4$, and $\varepsilon_4 = \frac{d}{dt} \left[R_\alpha(\theta) J(q) \left(\hat{S}_q + \Delta J_{Rinv} \dot{x}_r \right) \right]$. Thus, we obtain the sliding condition if $\gamma_s > \varepsilon_4$, such as $\mu_s > 0$ of (56) guarantee the sliding mode at $S_{s\delta} = 0$ at $t_s = \frac{|S_{s\delta}(t_0)|}{\mu_s}$. However, notice that for any initial condition $S_{s\delta}(t_0) = 0$, then $t_s = 0$, which implies that the sliding mode at $S_{s\delta}(t) = 0$ is guaranteed for all time.

Part II.b: Sliding modes for the force subspace. Similarly, if we multiply (54) by $(J_\varphi J_\varphi^T(q))^{-1}$, we obtain

$$(J_\varphi J_\varphi^T(q))^{-1} J_\varphi \hat{S}_q = -\beta J_\varphi J_\varphi^T \{S_{vF}\} \quad (57)$$

$$J_\varphi^\#(q) \hat{S}_q = S_{F\delta} + \gamma_{F1} \int_{t_0}^t S_{F\delta} + \gamma_{F2} \int_{t_0}^t \text{sign}(S_{F\delta}) \quad (58)$$

where $J_\varphi^\#(q) = (-\beta J_\varphi J_\varphi^T(q))^{-1} J_\varphi$. Derivating (58) and multiply it by $S_{F\delta}^T$ becomes

$$S_{F\delta}^T \dot{S}_{F\delta} = -\gamma_{F2} |S_{F\delta}| - \gamma_{F1} S_{F\delta}^T S_{F\delta} + S_{F\delta}^T \frac{d}{dt} \left(J_\varphi^\#(q) \hat{S}_q \right) \quad (59)$$

$$\leq -\gamma_{F2} |S_{F\delta}| - \gamma_{F1} \|S_{F\delta}\|^2 + |S_{F\delta}| \frac{d}{dt} \left(J_\varphi^\#(q) \hat{S}_q \right) \quad (60)$$

$$\leq -\mu_F |S_{F\delta}| - \gamma_{F1} \|S_{F\delta}\|^2 \quad (61)$$

where $\mu_F = \gamma_F - \varepsilon_5$, and $\varepsilon_5 = \frac{d}{dt} \left[(J_\varphi J_\varphi^T(q))^{-1} J_\varphi \hat{S}_q \right]$. If $\gamma_F > \varepsilon_5$, then a sliding mode at $S_{F\delta}(t) = 0$ is induced at $t_f \leq \frac{|S_{F\delta}(t_0)|}{\mu_F}$, but $S_{F\delta}(t_0) = 0$, thus $S_{F\delta}(t) = 0$ is guaranteed $\forall t$.

Part III: Exponential convergence of tracking errors.

Part III.a: Visual tracking errors. Since a sliding mode exists for all time at $S_{s\delta}(t) = 0$, then, we have

$$S_s = S_{sd} \forall t \rightarrow \Delta \dot{x}_s = -\alpha \Delta x_s + S_s(t_0) e^{-\kappa_s t}$$

this implies that the visual tracking errors locally tends to zero exponentially fast, this is $x_s \rightarrow x_{sd}$, $\dot{x}_s \rightarrow \dot{x}_{sd}$, implying that the robot end-effector converges to the desired image x_{sd} , with given velocity \dot{x}_{sd} .

Part III.b: Force tracking errors. Since a sliding mode at $S_{F\delta}(t) = 0$ is induced for all time, this means $\Delta F =$

$\Delta F(t_0) e^{-\kappa_F t}$. Moreover, in [10] it is shown that the convergence of force tracking errors arises, thus $\lambda \rightarrow \lambda_d$ exponentially fast. **QED.**

Theorem 2 : Proof. With the very same Lyapunov function of *Theorem 1*, we obtain the following time derivative, along trajectories of the closed loop of (44)-(45) and (43),

$$\dot{V} \leq -K_d \|\hat{S}_q\|_2^2 - \eta\beta \|S_{vF}\| + \|\hat{S}_q\| \psi - \dot{V}_f \quad (62)$$

where

$$\begin{aligned} \dot{V}_f &= \sigma_0 \hat{S}_q^T [z + \sigma_{01} \tanh(\xi_f \hat{S}_q)] - \sigma_{01} \hat{S}_q [-zh(\dot{x}) \\ &+ \alpha_0^{-1} \sigma_{01} |\dot{x}| \tanh(\xi_f \hat{S}_q)]. \end{aligned} \quad (63)$$

In [11], [12] it was proved that $\dot{V}_f > 0$, and $|\dot{V}_f| < \varepsilon_4$, $\varepsilon_4 > 0$. Then, \dot{V}_f is positive definite outside the hyperball $\rho_0 = \rho_0(\hat{S}_q) = \{\hat{S}_q | V_f \leq 0\}$ with $\|\rho_0\| \leq \rho$, for $\rho > 0$. Thus, if we choose ξ_f large enough, preventing that the mechatronic system does not introduce high frequency from the term $\tanh(\xi_f \hat{S}_q)$, then (62) becomes

$$\dot{V} \leq -\hat{S}_q^T K_f \hat{S}_q - \hat{S}_q^T mKZ + \rho_0. \quad (64)$$

Afterwards, we proceed exactly as in proof of theorem 1, and it is therefore omitted. **QED.**